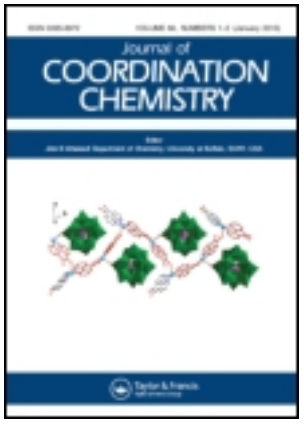

Journal of Coordination Chemistry
Publication details, including instructions for authors and subscription information:
http://www.tandfonline.com/loi/gcoo20

Nuclease activity of redox/non-redox active binuclear transition metal mixed-polypyridine complexes: $[M_2(1,4\text{-tpbd})(diimine)_2(H_2O)_2]^{4+}$, M = Zn, Co, Ni, Cd, diimine = phen, bpy, dafo

Dong-Dong Li[a] & Zun-Wei Tao[a]
[a] Tianjin Institute of Medical and Pharmaceutical Sciences, Tianjin, China
Published online: 10 Dec 2013.

Journal of Coordination Chemistry, 2013
Vol. 66, No. 24, 4237–4254, http://dx.doi.org/10.1080/00958972.2013.866655

Nuclease activity of redox/non-redox active binuclear transition metal mixed-polypyridine complexes: $[M_2(1,4\text{-tpbd})(diimine)_2(H_2O)_2]^{4+}$, M = Zn, Co, Ni, Cd, diimine = phen, bpy, dafo

DONG-DONG LI* and ZUN-WEI TAO

Tianjin Institute of Medical and Pharmaceutical Sciences, Tianjin, China

(*Received 10 September 2013; accepted 31 October 2013*)

Seven new transition metal complexes formulated as $[M_2(1,4\text{-tpbd})(diimine)_2(H_2O)_2]^{4+}$ [M = Zn, Co, Ni, Cd; 1,4-tpbd = *N*,*N*,*N*′,*N*′-tetrakis(2-pyridylmethyl)benzene-1,4-diamine; diimine is a N,N-donor heterocyclic base like 1,10-phenanthroline (phen), 2,2′-bipyridine (bpy), 4,5-diazafluoren-9-one (dafo)] have been synthesized and structurally characterized by X-ray crystallography: $[Zn_2(1,4\text{-tpbd})(phen)_2(H_2O)_2]^{4+}$ (**1**), $[Zn_2(1,4\text{-tpbd})(bpy)_2(H_2O)_2]^{4+}$ (**2**), $[Co_2(1,4\text{-tpbd})(phen)_2(H_2O)_2]^{4+}$ (**3**), $[Ni_2(1,4\text{-tpbd})(phen)_2(H_2O)_2]^{4+}$ (**4**), $[Ni_2(1,4\text{-tpbd})(bpy)_2(H_2O)_2]^{4+}$ (**5**), $[Ni_2(1,4\text{-tpbd})(dafo)_2(H_2O)_2]^{4+}$ (**6**) and $[Cd_2(1,4\text{-tpbd})(phen)_2(H_2O)_2]^{4+}$ (**7**). Single crystal diffraction reveals that the metals in the complexes are all in a distorted octahedral geometry. The interactions of the seven complexes with calf thymus DNA (CT-DNA) have been investigated by UV absorption, fluorescence, circular dichroism spectroscopy and viscosity measurements. The apparent binding constants (K_{app}) are calculated to be 5.2×10^5 M^{-1} for **1**, 1.05×10^5 M^{-1} for **2**, 5.76×10^5 M^{-1} for **3**, 4.57×10^5 M^{-1} for **4**, 1.29×10^5 M^{-1} for **5**, 1.7×10^5 M^{-1} for **6**, 2.53×10^5 M^{-1} for **7**, the binding propensity to the calf thymus DNA in the order: **3** (Co-phen) > **1** (Zn-phen) > **4** (Ni-phen) > **7** (Cd-phen) > **6** (Ni-dafo) > **5** (Ni-bpy) > **2** (Zn-bpy). Furthermore, these complexes display efficient oxidative cleavage of supercoiled DNA; the Zn(II)/H_2O_2 and Cd(II)/H_2O_2 systems efficiently cleave DNA attributed to the peroxide ion coordinated to the Zn(II) and Cd(II), which enhanced their nucleophilicity, this is rare.

Keywords: Mixed-polypyridine complexes; DNA binding; Oxidative cleavage

1. Introduction

Artificial metallonucleases have received attention for their diverse application in gene regulation, mapping of protein and DNA interactions, probing of DNA specific structures, and in cancer therapy [1–4]. Transition metal complexes of Cu(II), Co(II), Ni(II), Fe(III), Mn(II) and Cr(III) have been reported to mediate DNA oxidation in the presence of oxidants or reductants or without any assistant agents [5–12]. Many of them utilize the redox properties of the metal and dioxygen to produce reactive oxygen (ROS) or metal-oxo species (RMOS) that oxidize DNA, yielding direct strand scission or base modification [13]. Several typical mononuclear complexes as nucleolytic agents are $[Fe(EDTA)]^{2-}$ (EDTA = ethylenediaminetetraacetate) [14], $[Cu(OP)_2]^+$ (OP = 1,10-phenanthroline) [15],

*Corresponding author. Email: lidongdong2010@163.com

Fe-BLM (BLM = bleomycin) [16, 17], metalloporphyrins [18], Ni-peptides [19] and metal salen [salen = *N*,*N*-ethylenebis(salicylidene aminato)] [20]. Recently, the multinuclear complexes have attracted more interest as metallonucleases for the potential cooperative effects between the metal centers [21, 22]; they show higher oxidative DNA-cleavage activity than that of mononuclear complexes. The DNA-cleavage ability of metallonucleases can be affected by metal centers, ligands, co-factors as well as external agents, pH, ion strength, temperature and reaction time. Therein, the metal centers largely control the redox potential, the formation of reactive species and DNA binding ability. Ligands act as the unit of functional regulation. For non-redox active Zn(II) complexes, most show hydrolytic DNA cleavage; oxidative DNA cleavage by Zn(II) complexes is rare. For example, Reedjik *et al.* [23, 24] have reported some ligand-based Zn(II) complexes showing oxidative DNA cleavage, possibly due to the involvement of a non-diffusible phenoxyl radical mechanism. For Cd(II) complexes, the field of their potential anticancer activity is explored scarcely, which is apparently caused by the known toxic properties of cadmium [25, 26], but recently Cd(II) has been found to react with nucleobases, nucleic metallothionein and plasmid DNA causing extensive damage to these targets [27, 28]. Several Cd(II) complexes have been found to display a potential anticancer character [29–31]. Many studies suggest that DNA is the primary intracellular target of metal-based antitumor drugs such as cisplatin. The interaction between small molecules and DNA can cause DNA damage in cancer cells, blocking the division of cancer cells and resulting in cell death. Therefore, metal complexes which exhibit DNA binding and cleavage properties can be candidates suitable for investigation *in vitro* cytotoxicity.

In our study, we have synthesized and characterized a family of transition metal complexes with 1,4-tpbd ligand and coligand (shown in scheme 1), and studied the DNA binding and nuclease activity. The interaction between calf thymus DNA and complex was investigated by UV absorption, fluorescence spectroscopy, circular dichroism spectroscopy and viscosity; the DNA cleavage induced by these complexes is also demonstrated. The investigation indicates that Zn(II)/H_2O_2 and Cd(II)/H_2O_2 systems have the highest DNA-cleavage efficiency through oxidative mechanism, which is attributed to the peroxide ion coordinated to the Zn(II) and Cd(II) ions, which enhanced their nucleophilicity. The effective nuclease activity of Co(II) and Ni(II) complexes is attributed to reactive oxygen species formed by redox active metal ions with molecular oxygen or hydrogen peroxide.

2. Experimental

Caution: Although no problems were encountered in this work, transition-metal perchlorate salts are potentially explosive and should thus be prepared in small quantities and handled with care.

2.1. *Materials and instrumentation*

The 1,4-tpbd ligand was synthesized according to the procedure [32]. Ethidium bromide (EB), calf thymus DNA (CT-DNA) and pBR322 plasmid DNA were from Sigma. Tris-HCl buffer solution was prepared using deionized sonicated triply-distilled water. All other chemicals used were of analytical grade. Solutions of the complexes and other reagents used for strand scission were prepared freshly in triply-distilled water before use. Solvents used in this research were purified by standard procedures.

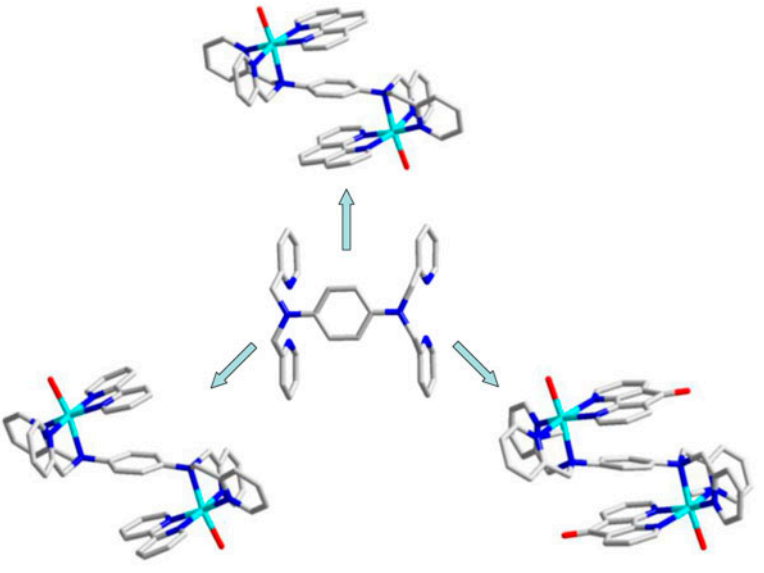

Scheme 1. Structures of complexes with 1,4-tpbd ligand and coligand of phen, bpy and dafo.

Elemental analyses for C, H and N were obtained on a Perkin–Elmer analyzer model 240. Infrared spectroscopy on KBr pellets was performed on a Bruker Vector 22 FT-IR spectrophotometer from 4000–400 cm^{-1}. The electronic spectra were measured on a JASCO V-570 spectrophotometer. The fluorescence spectral data were obtained on a MPF-4 fluorescence spectrophotometer at room temperature. The CD spectra of CT-DNA in the presence or absence of complexes were performed on a JASCO-J715 spectropolarimeter at room temperature. The gel imaging and documentation DigiDoc-It System were assessed using Labworks Imaging and Analysis Software (UVI, England).

2.2. *Preparation of complexes*

2.2.1. Synthesis of $[Zn_2(1,4\text{-tpbd})(phen)_2(H_2O)_2](ClO_4)_4\cdot 1.5CH_3OH$ (1). To a methanolic solution (10 mL) of 1,4-tpbd (0.1 mM, 0.0473 g) was added dropwise an aqueous solution (5 mL) of $Zn(ClO_4)_2\cdot 6H_2O$ (0.2 mM, 0.0745 g). The mixture was refluxed for 3 h in the presence of air, then phen (0.2 mM, 0.0396 g) was added and refluxed for an additional 2 h and filtered. After several days, light yellow block crystals of **1** suitable for X–ray structure analysis were obtained by slow evaporation of the filtrate, collected by filtration, washed with diethyl ether and dried in air. Yield 37% (based on the zinc salts). Elemental analysis data: Calcd (%) for $C_{55.5}H_{54}Cl_4N_{10}O_{19.5}Zn_2$ (1445.67): C, 46.11; H, 3.77; N, 9.69. Found (%): C, 46.08; H, 3.80; N, 9.65. IR (KBr, ν, cm^{-1}): 1606, 1619, 1488, 1472, 1209, 1089, 1019, 853, 774, 728, 626. UV–Vis: λ/nm (ε/dm^3 M^{-1} cm^{-1}): 221 (145204), 266 (56582).

2.2.2. Synthesis of $[Zn_2(1,4\text{-tpbd})(bpy)_2(H_2O)_2](ClO_4)_4$ (2). Complex **2** was prepared in a similar way to that of **1** except for bpy (0.2 mM, 0.0312 g) instead of phen (0.2 mM, 0.0396 g). The mixture was stirred for 5 h at room temperature and filtered. After several

days, light yellow block crystals of **2** suitable for X–ray structure analysis were obtained by slow evaporation of the filtrate, collected by filtration, washed with diethyl ether and dried in air. Yield 35% (based on the zinc salts). Elemental analysis data: Calcd (%) for $C_{50}H_{52}Cl_4N_{10}O_{20}Zn_2$ (1385.56): C, 43.34; H, 3.78; N, 10.11. Found (%): C, 43.31; H, 3.82; N, 10.08. IR (KBr, ν, cm^{-1}): 1606, 1518, 1476, 1440, 1210, 1086, 1019, 771, 626. UV–Vis: λ/nm (ε/dm^3 M^{-1} cm^{-1}): 227 (134694), 295 (22194).

2.2.3. Synthesis of $[Co_2(1,4\text{-tpbd})(phen)_2(H_2O)_2](ClO_4)_4\cdot CH_3OH\cdot H_2O$ (3). Complex **3** was prepared in a similar way to that of **1** except for $Co(ClO_4)_2\cdot 6H_2O$ instead of $Zn(ClO_4)_2\cdot 6H_2O$. After addition of phen, the mixture was stirred for 12 h at room temperature and filtered. After several days, orange block crystals of **3** suitable for X–ray structure analysis were obtained by slow evaporation of the filtrate, collected by filtration, washed with diethyl ether and dried in air. Yield 33% (based on the cobalt salts). Elemental analysis data: Calcd (%) for $C_{55}H_{52.5}Cl_4N_{10}O_{19.25}Co_2$ (1421.19): C, 46.48; H, 3.72; N, 9.86. Found (%): C, 46.45; H, 3.76; N, 9.85. IR (KBr, ν, cm^{-1}): 1606, 1519, 1485, 1427, 1086, 1020, 853, 778, 728, 627. UV–Vis: λ/nm (ε/dm^3 M^{-1} cm^{-1}): 221 (166837), 266 (79439).

2.2.4. Synthesis of $[Ni_2(1,4\text{-tpbd})(phen)_2(H_2O)_2](ClO_4)_4$ (4). Complex **4** was prepared in a similar way to that of **1** except for $Ni(ClO_4)_2\cdot 6H_2O$ instead of $Zn(ClO_4)_2\cdot 6H_2O$. After addition of phen, the mixture was stirred for 12 h at room temperature and filtered. After several days, light purple block crystals of **4** suitable for X–ray structure analysis were obtained by slow evaporation of the filtrate, collected by filtration, washed with diethyl ether and dried in air. Yield 38% (based on the nickel salts). Elemental analysis data: Calcd (%) for $C_{54}H_{48}Cl_4N_{10}O_{18}Ni_2$ (1384.24): C, 46.86; H, 3.50; N, 10.12. Found (%): C, 46.83; H, 3.55; N, 10.10. IR (KBr, ν, cm^{-1}): 1607, 1519, 1488, 1428, 1206, 1114, 926, 860, 783, 728, 626. UV–Vis: λ/nm (ε/dm^3 M^{-1} cm^{-1}): 221 (166837), 266 (79439). UV–Vis: λ/nm (ε/dm^3 M^{-1} cm^{-1}): 223 (165204), 266 (75000).

2.2.5. Synthesis of $[Ni_2(1,4\text{-tpbd})(bpy)_2(H_2O)_2](ClO_4)_4$ (5). To a methanolic solution (10 mL) of 1,4-tpbd (0.1 mM, 0.0473 g) was added dropwise an aqueous solution (5 mL) of $Ni(ClO_4)_2\cdot 6H_2O$ (0.2 mM, 0.0731 g). The mixture was refluxed for 4 h in the presence of air, then bpy (0.2 mM, 0.0312 g) was added and refluxed for an additional 2 h and filtered. After several days, green block crystals of **5** suitable for X–ray structure analysis were obtained by slow evaporation of the filtrate, collected by filtration, washed with diethyl ether and dried in air. Yield 37% (based on the nickel salts). Elemental analysis data: Calcd (%) for $C_{50}H_{48}Cl_4N_{10}O_{18}Ni_2$ (1336.16): C, 44.95; H, 3.62; N, 10.48. Found (%): C, 44.92; H, 3.65; N, 10.45. IR (KBr, ν, cm^{-1}): 1607, 1573, 1517, 1476, 1443, 1089, 1109, 1023, 928, 771, 736, 626. UV–Vis: λ/nm (ε/dm^3 M^{-1} cm^{-1}): 223 (160459), 299 (33980).

2.2.6. Synthesis of $[Ni_2(1,4\text{-tpbd})(dafo)_2(H_2O)_2](ClO_4)_4\cdot 6H_2O$ (6). Complex **6** was prepared in a similar way to that of **5** except for dafo instead of bpy, filtered. After several days, green block crystals of **6** suitable for X–ray structure analysis were obtained by slow evaporation of the filtrate, collected by filtration, washed with diethyl ether and dried in air. Yield 38% (based on the nickel salts). Elemental analysis data: Calcd (%) for $C_{52}H_{52}Cl_4N_{10}O_{26}Ni_2$ (1492.22): C, 41.86; H, 3.51; N, 9.39. Found (%): C, 41.83; H, 3.58;

N, 10.35. IR (KBr, ν, cm^{-1}): 1734, 1608, 1586, 1509, 1441, 1417, 1089, 764, 627. UV–Vis: λ/nm (ε/dm^3 M^{-1} cm^{-1}): 219 (157143), 310 (15153).

2.2.7. Synthesis of $[Cd_2(1,4\text{-tpbd})(phen)_2(H_2O)_2](ClO_4)_4$ (7). Complex **7** was prepared in a similar way to that of **1** except for $Cd(ClO_4)_2{\cdot}6H_2O$ instead of $Zn(ClO_4)_2{\cdot}6H_2O$, filtered. After several days, light yellow crystals of **7** suitable for X–ray structure analysis were obtained by slow evaporation of the filtrate, collected by filtration, washed with diethyl ether and dried in air. Yield 30% (based on the cadmium salts). Elemental analysis data: Calcd (%) for $C_{54}H_{56}Cl_4N_{10}O_{18}Cd_2$ (1499.73): C, 43.25; H, 3.76; N, 9.34. Found (%): C, 43.20; H, 3.79; N, 9.31. IR (KBr, ν, cm^{-1}): 1518, 1427, 1144, 1089, 848, 774, 728, 625. UV–Vis: λ/nm (ε/dm^3 M^{-1} cm^{-1}): 221 (163163), 265 (109643).

2.3. *X-ray crystallography*

Single crystals of **1**–**7** were used for X-ray diffraction analyses by mounting on the tip of a glass fiber in air using a Bruker SMART CCD 1000 diffractometer. Diffraction intensities for the complexes were collected by using the ω-scan technique. The structures were solved by direct methods using SHELXS-97 [33] and subsequent Fourier difference techniques, and refined anisotropically by full-matrix least-squares on F^2 using SHELXL-97 [34]. All non-hydrogen atoms were refined anisotropically and all hydrogens were located in the Fourier difference maps. Further crystallographic data and experimental details for structural analyses of **1**–**7** are summarized in table 1. Selected bond distances and angles are listed in table 2.

Crystallographic data for **1**–**7** have been deposited with the Cambridge Crystallographic Data Centre as supplementary publication CCDC reference numbers 939559, 939560, 939561, 939562, 939563, 939564 and 939565, respectively. Any inquiries relating to the data can be e-mailed to deposit@ccdc.cam.ac.uk.

2.4. *DNA-binding studies*

Using the electronic absorption spectral method, the relative binding of complex to calf thymus (CT-DNA) was studied in 5 mM Tris-HCl/50 mM NaCl buffer (pH = 7.2). The solution of calf thymus (CT-DNA) gave a ratio of UV absorbance at 260 nm and 280 nm, A_{260}/A_{280}, of 1.8–1.9, indicating that the calf thymus DNA (CT-DNA) was sufficiently free of proteins [35]. The stock solution of calf thymus (CT-DNA) was prepared in Tris-HCl/NaCl buffer (pH = 7.2, stored at 4 °C and used when not more than 4 days). The concentration of calf thymus (CT-DNA) was determined from its absorption intensity at 260 nm with a molar extinction coefficient of 6600 $M^{-1}cm^{-1}$ [36]. The absorption spectra of **1**–**7** binding to calf thymus (CT-DNA) was performed by increasing amounts of calf thymus (CT-DNA) to **1**–**7** in 5 mM Tris-HCl/50 mM NaCl buffer (pH = 7.2).

By the fluorescence spectral method, the relative binding of **1**–**7** to calf thymus (CT-DNA) was studied with an EB-bound calf thymus (CT-DNA) solution in 5 mM Tris-HCl/50 mM NaCl buffer (pH = 7.2). Fluorescence intensities at 602 nm (510 nm excitation) were measured at different complex concentrations. The experiment was carried out by titrating **1**–**7** into EB–bound calf thymus (CT-DNA) solution ([EB] = 5×10^{-5} M, [CT-DNA] = 5×10^{-5} M).

Table 1. Crystallographic data and structure refinement parameters for **1**–**7**.

Complex	**1**	**2**	**3**	**4**	**5**	**6**	**7**
Empirical formula	$C_{55.5}H_{54}Cl_4N_{10}O_{19.5}Zn_2$	$C_{50}H_{52}Cl_4N_{10}O_{20}Zn_2$	$C_{55}H_{52.5}Cl_4Co_2N_{10}O_{19.25}$	$C_{54}H_{48}Cl_4N_{10}Ni_2O_{18}$	$C_{50}H_{48}Cl_4N_{10}Ni_2O_{18}$	$C_{52}H_{52}Cl_4N_{10}Ni_2O_{26}$	$C_{54}H_{56}Cd_2Cl_4N_{10}O_{18}$
M_r	1445.63	1385.56	1421.19	1384.24	1336.16	1492.22	1499.73
Crystal system	Triclinic	Orthorhombic	Triclinic	Monoclinic	Monoclinic	Triclinic	Triclinic
Space group	*P-1*	*Pbca*	*P-1*	*P2/n*	*$P2_1/n$*	*P-1*	*P-1*
a (Å)	10.500(2)	17.4970(14)	10.614(14)	15.9299(16)	12.154(2)	11.232(2)	10.628(2)
b (Å)	12.040(2)	16.2821(12)	11.948(16)	10.4818(6)	15.464(3)	12.440(3)	12.132(2)
c (Å)	13.389(3)	20.7979(16)	13.356(18)	19.2559(15)	15.252(3)	13.061(3)	13.589(3)
α (°)	74.22(3)	90	72.67(2)	90	90	71.36(3)	78.03(3)
β (°)	87.21(3)	90	85.23(2)	118.057(6)	97.43(3)	70.95(3)	87.12(3)
γ (°)	67.80(3)	90	67.03(2)	90	90	64.87(3)	66.12(3)
V (Å^3)	1505.4(5)	5925.1(8)	1488(3)	2837.4(4)	2842.5(10)	1526.5(5)	1566.2(5)
Z, D_{Cacld} (mg/m^3)	1, 1.595	4, 1.553	1, 1.591	2, 1.620	2, 1.561	1, 1.623	1, 1.590
μ (mm^{-1})	1.058	1.072	0.822	0.936	0.931	0.886	0.926
F (000)	741	2840	731	1420	1809	938	656
θ Range (°)	1.90–25.02	1.96–25.02	1.93–25.02	2.28–27.88	3.00–25.01	3.22–25.25	3.07–25.25
Reflections collected	8716	29148	7450	20226	22985	13104	13480
Unique reflections	5259	5230	5163	6751	5012	5510	5655
R_{int}	0.0448	0.0360	0.0620	0.0381	0.0527	0.0369	0.0672
Goodness-of-fit on F^2	1.110	1.117	1.030	1.064	1.052	1.189	1.170
R_1/wR_2 [$I>2\sigma(I)$]	0.0700/0.2134	0.0637/0.1955	0.0838/0.1965	0.0459/0.1122	0.0724/0.1889	0.0823/0.2035	0.0791/0.1733
R_1/wR_2 (all data)	0.081/0.2226	0.0904/0.2315	0.1716/0.2462	0.0522/0.1165	0.0888/0.2021	0.0956/0.2103	0.1083/0.1855
$\Delta\rho_{max,min}$/(e Å^{-3})	1.228/−1.095	0.785/−0.493	0.699/−0.486	0.775/−1.007	1.081/−1.047	1.153/−0.904	0.617/−0.674

Table 2. Selected bond lengths (Å) and angles (°) for **1**–**7**.

Complex **1**							
Zn(1)–O(1)	2.098(4)	Zn(1)–N(1)	2.111(5)	Zn(1)–N(5)	2.124(4)	Zn(1)–N(3)	2.132(4)
Zn(1)–N(4)	2.158(4)	Zn(1)–N(2)	2.376(4)	Zn(1)···Zn(1A)	8.337(3)		
O(1)–Zn(1)–N(1)	100.01(17)	O(1)–Zn(1)–N(5)	92.31(17)	N(5)–Zn(1)–N(4)	78.37(18)	N(3)–Zn(1)–N(4)	170.53(15)
N(1)–Zn(1)–N(5)	164.03(18)	O(1)–Zn(1)–N(3)	95.64(17)	O(1)–Zn(1)–N(2)	171.76(15)	N(1)–Zn(1)–N(2)	78.34(16)
N(1)–Zn(1)–N(3)	91.03(17)	N(5)–Zn(1)–N(3)	97.88(17)	N(5)–Zn(1)–N(2)	90.85(16)	N(3)–Zn(1)–N(2)	76.39(15)
O(1)–Zn(1)–N(4)	93.22(16)	N(1)–Zn(1)–N(4)	90.74(17)	N(4)–Zn(1)–N(2)	94.87(15)		
Complex **2**							
Zn(1)–O(1)	2.088(4)	Zn(1)–N(3)	2.114(5)	Zn(1)–N(4)	2.160(5)	Zn(1)–N(2)	2.381(4)
Zn(1)–N(1)	2.145(5)	Zn(1)–N(5)	2.155(5)	Zn(1)···Zn(1A)	8.482(1)		
O(1)–Zn(1)–N(3)	94.45(19)	O(1)–Zn(1)–N(1)	95.60(19)	N(1)–Zn(1)–N(4)	91.8(2)	N(5)–Zn(1)–N(4)	76.3(2)
N(3)–Zn(1)–N(1)	96.13(19)	O(1)–Zn(1)–N(5)	94.5(2)	O(1)–Zn(1)–N(2)	167.29(18)	N(3)–Zn(1)–N(2)	77.83(17)
N(3)–Zn(1)–N(5)	93.9(2)	N(1)–Zn(1)–N(5)	165.18(19)	N(1)–Zn(1)–N(2)	75.46(16)	N(5)–Zn(1)–N(2)	96.10(16)
O(1)–Zn(1)–N(4)	96.16(19)	N(3)–Zn(1)–N(4)	166.1(2)	N(4)–Zn(1)–N(2)	93.17(17)		
Complex **3**							
Co(1)–N(4)	2.069(7)	Co(1)–N(3)	2.079(7)	Co(1)–O(1)	2.086(6)	Co(1)–N(5)	2.122(7)
Co(1)–N(2)	2.273(7)	Co(1)–N(1)	2.079(7)	Co(1)···Co(1A)	8.141(8)		
N(4)–Co(1)–N(3)	97.9(3)	N(4)–Co(1)–N(1)	166.0(3)	N(1)–Co(1)–N(5)	90.6(3)	O(1)–Co(1)–N(5)	91.5(2)
N(3)–Co(1)–N(1)	92.2(2)	N(4)–Co(1)–O(1)	90.9(3)	N(4)–Co(1)–N(2)	92.4(3)	N(3)–Co(1)–N(2)	78.0(2)
N(3)–Co(1)–O(1)	94.9(2)	N(1)–Co(1)–O(1)	98.0(3)	N(1)–Co(1)–N(2)	80.1(3)	O(1)–Co(1)–N(2)	172.5(2)
N(4)–Co(1)–N(5)	78.3(3)	N(3)–Co(1)–N(5)	172.6(2)	N(5)–Co(1)–N(2)	95.7(2)		
Complex **4**							
Ni(1)–N(2)	2.0621(19)	Ni(1)–N(1)	2.0677(19)	Ni(1)–N(5)	2.1066(19)	Ni(1)–N(3)	2.2211(19)
Ni(1)–O(9)	2.0759(18)	Ni(1)–N(4)	2.089(2)	Ni(1)···Ni(1A)	8.381(8)		
N(2)–Ni(1)–N(1)	91.20(8)	N(2)–Ni(1)–O(9)	93.55(8)	O(9)–Ni(1)–N(5)	91.79(7)	N(4)–Ni(1)–N(5)	79.23(8)
N(1)–Ni(1)–O(9)	94.39(8)	N(2)–Ni(1)–N(4)	169.27(8)	N(2)–Ni(1)–N(3)	82.16(7)	N(1)–Ni(1)–N(3)	78.79(7)
N(1)–Ni(1)–N(4)	95.92(8)	O(9)–Ni(1)–N(4)	93.89(7)	O(9)–Ni(1)–N(3)	171.81(7)	N(4)–Ni(1)–N(3)	91.35(7)
N(2)–Ni(1)–N(5)	92.82(7)	N(1)–Ni(1)–N(5)	172.40(8)	N(5)–Ni(1)–N(3)	95.37(7)		
Complex **5**							
Ni(1)–N(3)	2.054(4)	Ni(1)–N(1)	2.056(4)	Ni(1)–O(9)	2.089(4)	Ni(1)–N(2)	2.216(4)
Ni(1)–N(4)	2.076(4)	Ni(1)–N(5)	2.083(4)	Ni(1)···Ni(1A)	8.241(2)		
N(3)–Ni(1)–N(1)	94.79(18)	N(3)–Ni(1)–N(4)	94.92(19)	N(5)–Ni(1)–O(9)	90.1(2)	N(3)–Ni(1)–N(2)	80.84(16)
N(1)–Ni(1)–N(4)	167.88(18)	N(1)–Ni(1)–N(5)	91.42(18)	N(1)–Ni(1)–N(2)	77.99(15)	N(4)–Ni(1)–N(2)	96.44(15)
N(4)–Ni(1)–N(5)	78.62(19)	N(3)–Ni(1)–O(9)	91.7(2)	N(5)–Ni(1)–N(2)	98.10(16)	O(9)–Ni(1)–N(2)	169.54(18)
N(1)–Ni(1)–O(9)	95.47(17)	N(4)–Ni(1)–O(9)	91.47(18)	N(3)–Ni(1)–N(5)	173.33(17)		

(*Continued*)

Table 2. (*Continued*).

Complex **6**							
Ni(1)–O(1)	2.065(4)	Ni(1)–N(1)	2.056(5)	Ni(1)–N(4)	2.176(4)	Ni(1)–N(5)	2.210(5)
Ni(1)–N(2)	2.056(5)	Ni(1)–N(3)	2.204(4)	Ni(1)···Ni(1A)	8.141(8)		
O(1)–Ni(1)–N(1)	94.16(18)	O(1)–Ni(1)–N(2)	98.09(18)	N(2)–Ni(1)–N(3)	81.21(17)	N(4)–Ni(1)–N(3)	90.77(17)
N(1)–Ni(1)–N(2)	98.35(18)	O(1)–Ni(1)–N(4)	91.30(18)	O(1)–Ni(1)–N(5)	89.24(18)	N(1)–Ni(1)–N(5)	171.56(18)
N(1)–Ni(1)–N(4)	90.68(18)	N(2)–Ni(1)–N(4)	166.42(16)	N(2)–Ni(1)–N(5)	88.80(17)	N(4)–Ni(1)–N(5)	81.50(17)
O(1)–Ni(1)–N(3)	172.36(16)	N(1)–Ni(1)–N(3)	78.46(17)	N(3)–Ni(1)–N(5)	98.34(16)		
Complex **7**							
Cd(1)–O(1)	2.280(6)	Cd(1)–N(5)	2.323(6)	Cd(1)–N(4)	2.342(6)	Cd(1)–N(2)	2.562(6)
Cd(1)–N(3)	2.326(6)	Cd(1)–N(1)	2.333(6)	Cd(1)···Cd(1A)	8.504(3)		
O(1)–Cd(1)–N(5)	99.5(3)	O(1)–Cd(1)–N(3)	100.2(3)	N(3)–Cd(1)–N(4)	90.4(2)	N(1)–Cd(1)–N(4)	164.85(19)
N(5)–Cd(1)–N(3)	155.2(2)	O(1)–Cd(1)–N(1)	96.1(2)	O(1)–Cd(1)–N(2)	165.4(2)	N(5)–Cd(1)–N(2)	90.6(2)
N(5)–Cd(1)–N(1)	100.4(2)	N(3)–Cd(1)–N(1)	92.4(2)	N(3)-Cd(1)–N(2)	73.3(2)	N(1)–Cd(1)–N(2)	71.6(2)
O(1)–Cd(1)–N(4)	98.0(2)	N(5)–Cd(1)–N(4)	71.9(2)	N(4)–Cd(1)–N(2)	95.10(19)		

The CD spectra of calf thymus (CT-DNA) in the presence and absence of **1**–**7** were collected in Tris-HCl buffer (pH = 7.2) containing 50 mM NaCl. All CD experiments were performed on a JASCO-J715 spectropolarimeter at room temperature from 350 to 230 nm.

Viscosity experiments were carried out using an Ubbelodhe viscometer maintained at a constant temperature at 37.0 ± 0.1 °C in a thermostatic water-bath. Flow time was measured with a digital stopwatch, and each sample was measured three times, and an average flow time was calculated. Data were presented as $(\eta/\eta_0)^{1/3}$ *versus* [complex]/[DNA], where η is the viscosity of calf thymus (CT-DNA) in the presence of complex and η_0 is the viscosity of calf thymus (CT-DNA) alone in 5 mM Tris buffer medium. The viscosity values were calculated from the observed flow time of calf thymus (CT-DNA) containing solutions (t), duly corrected for that of the buffer alone (t_0), $\eta = (t - t_0)$. According to Cohen and Eisenberg [37], the relation between the relative solution viscosity (η/η_0) and contour length (L/L_0) is given by the following equation: $L/L_0 = (\eta/\eta_0)^{1/3}$, where L_0 denotes the apparent molecular length in the absence of the metal complex.

2.5. *DNA cleavage and mechanism studies*

The DNA cleavage experiment was done by agarose gel electrophoresis. The reaction was carried out following a literature method [38]. Bands were visualized by UV light and photographed. The resolved bands were visualized by EB staining and were then quantified. A correction factor of 1.22 was utilized to account for the decreased ability of EB to intercalate into Form I DNA compared with Form II [39].

Cleavage mechanistic investigation of pBR322 DNA was carried out in the presence of standard radical scavengers and reaction inhibitors. These reactions were carried out by adding scavengers of DMSO, EtOH, NaN_3, L-Histidine, KI, superoxide dismutase enzyme (SOD), catalase, methyl green and SYBR Green to pBR322 DNA prior to the addition of complex. Cleavage was initiated by the addition of complex and quenched with 2 μL of loading buffer. Further analysis was carried out by the above standard method.

3. Results and discussion

3.1. *X-ray structure characterization*

Complexes **1**–**7** have been structurally characterized by X-ray crystallography (figure 1). They consist of a similar cation structure, $[M_2(1,4\text{-tpbd})(X)_2(H_2O)_2]^{4+}$. The metal atoms in complexes all exhibit a distorted octahedral environment with N_5O donor set derived from three ligand N atoms, two coligand N atoms and one water O atom; the water O atom and the nitrogen atom from a tertiary amino-N atom occupy apical positions. A *trans* arrangement is evident in complexes due to crystal-packing effects, with the coligands like phen, bpy and dafo paralleling with phenyl ring. The dihedral angles between the phenyl ring and coligand for **1**–**7** are 0.063°, 0.069°, 0.066°, 0.084°, 0.041°, 0.063° and 0.055°, respectively. The distance between metal ions in each binuclear complex is larger than the previous binuclear complex $[Cu_2(1,4\text{-tpbd})(H_2O)_4]^{4+}$ (8.099 Å) [40] due to steric effect from the coligand.

3.2. *DNA binding studies*

Complexes **1**–**7** can dissolve in water, which facilitates the investigation of the complexes in aqueous solution. UV absorption, fluorescence spectroscopy, circular dichroism

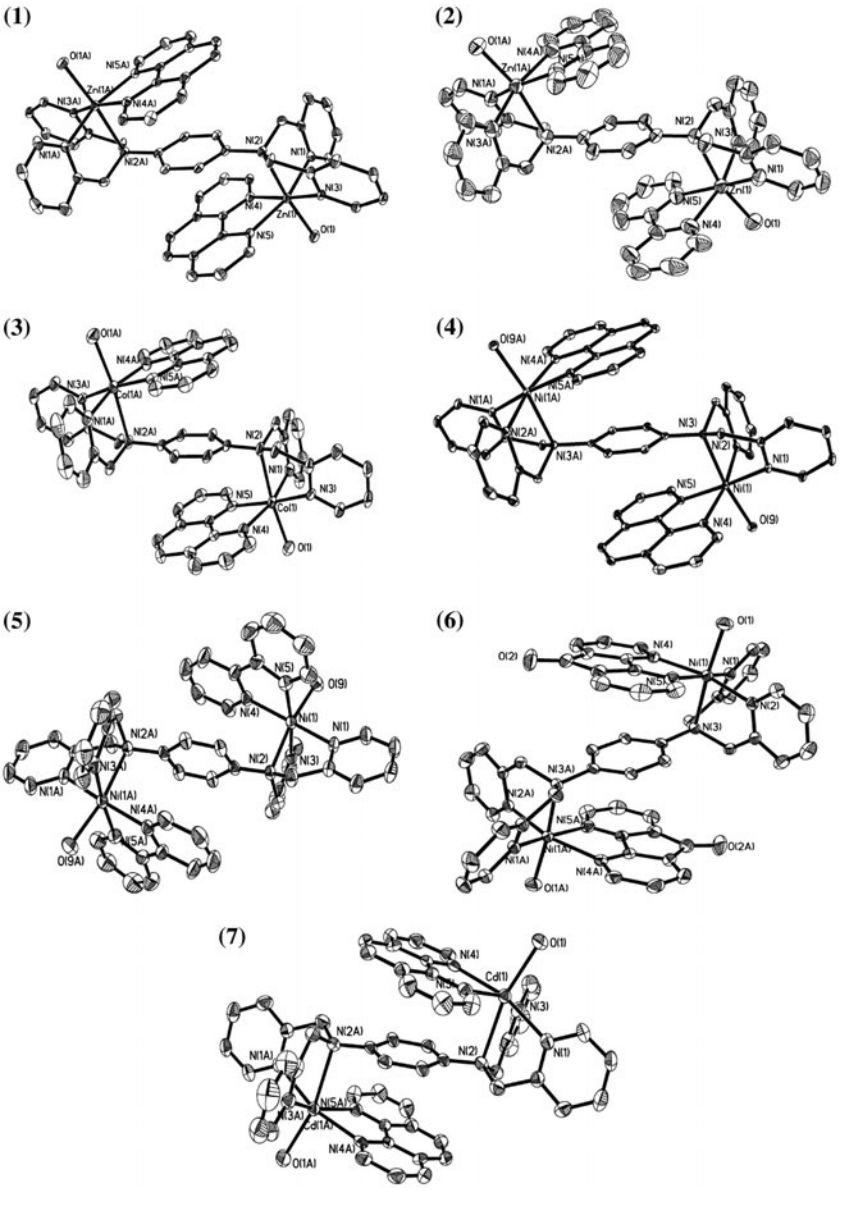

Figure 1. (**1**) ORTEP view of $[Zn_2(1,4\text{-tpbd})(phen)_2(H_2O)_2]^{4+}$. Thermal ellipsoids are drawn at 30% probability level. The "A" labeled atoms are at equivalent positions $(-x+2, -y+1, -z+1)$; (**2**) ORTEP view of $[Zn_2(1,4\text{-tpbd})(bpy)_2(H_2O)_2]^{4+}$. Thermal ellipsoids are drawn at 30% probability level. The "A" labeled atoms are at equivalent positions $(-x, -y+1, -z)$; (**3**) ORTEP view of $[Co_2(1,4\text{-tpbd})(phen)_2(H_2O)_2]^{4+}$. Thermal ellipsoids are drawn at 30% probability level. The "A" labeled atoms are at equivalent positions $(-x+2, -y+1, -z+1)$; (**4**) ORTEP view of $[Ni_2(1,4\text{-tpbd})(phen)_2(H_2O)_2]^{4+}$. Thermal ellipsoids are drawn at 30% probability level. The "A" labeled atoms are at equivalent positions $(-x+1, -y, -z+1)$; (**5**) ORTEP view of $[Ni_2(1,4\text{-tpbd})(bpy)_2(H_2O)_2]^{4+}$. Thermal ellipsoids are drawn at 30% probability level. The "A" labeled atoms are at equivalent positions $(-x, -y+1, -z+2)$; (**6**) ORTEP view of $[Ni_2(1,4\text{-tpbd})(dafo)_2(H_2O)_2]^{4+}$. Thermal ellipsoids are drawn at 30% probability level. The "A" labeled atoms are at equivalent positions $(-x+2, -y+1, -z+2)$; (**7**) ORTEP view of $[Cd_2(1,4\text{-tpbd})(phen)_2(H_2O)_2]^{4+}$. Thermal ellipsoids are drawn at 30% probability level. The "A" labeled atoms are at equivalent positions $(-x, -y+1, -z+1)$.

spectroscopy, viscosity, and DNA cleavage experiments were all investigated in aqueous solution. Our work has approved the stability of this kind of complexes in aqueous solution by the ESMS results, which shows that the metal ion and ligand species exist as a whole entity like $[M_2(tpbd)(diimine)_2(H_2O)\ (OH)]^{3+}$ or $[M_2(tpbd)(diimine)_2(OH)_2]^{2+}$ [41].

3.2.1. Electronic absorption titration. DNA binding is the critical step for DNA cleavage in most cases. Therefore, the binding ability of the complex with DNA is characterized by measuring the effects on the UV spectroscopy and fluorescence spectra of calf thymus DNA (CT-DNA). A complex bound to DNA through intercalation is characterized by hypochromism in absorbance and red shift in wavelength, due to the intercalation mode involving a strong stacking interaction between the aromatic chromophore and the DNA base pairs [42]. The extent of hypochromism is commonly consistent with the strength of the intercalative interaction [43–45]. The absorption spectra of **1**–**7** in the absence and presence of calf thymus (CT-DNA) at different concentrations are given in figure S1 (see online supplemental material at http://dx.doi.org/10.1080/00958972.2013.866655). In the UV region, the complexes all exhibit two absorption bands, which are attributed to the π–π* transition. On increasing the calf thymus (CT-DNA) concentration, they all show hypochromism and red shift at maximum peak. The detailed parameters are shown in table S1, which suggest intercalation between the complexes and calf thymus (CT-DNA).

The intrinsic binding constants K_b were calculated to be $5.14 \times 10^4\ M^{-1}$ for **1**, $3.12 \times 10^4\ M^{-1}$ for **2**, $17.4 \times 10^4\ M^{-1}$ for **3**, $8.58 \times 10^4\ M^{-1}$ for **4**, $4.24 \times 10^4\ M^{-1}$ for **5**, $6.37 \times 10^4\ M^{-1}$ for **6**, and $15.9 \times 10^4\ M^{-1}$ for **7**, respectively. As seen in table S2, the K_b values are lower than that of the typical classic intercalator EB (EthBr, K_b, $4.94 \times 10^5\ M^{-1}$), but higher than those of binuclear Cu(II), Zn(II), Co(II) and Ni(II) complexes [46–48]. The better binding affinity of present binuclear complexes may be due to the coligand system for better stacking between the base pairs of DNA, as well as the 1,4-tpbd ligand. The K_b values of Co(II) and Ni(II) complexes are higher than those of mononuclear Co(II) complexes [49, 50], but lower than that of macrocyclic binuclear Ni(II) complex [51], which is attributed to formation of several hydrogen bonds between compound and DNA.

3.2.2. Fluorescence spectroscopic studies. No luminescence is observed for **1**–**7** at room temperature in aqueous solution, in any organic solvent examined, or in the presented CT-DNA. So the binding of the complexes to CT-DNA cannot be directly presented in the emission spectra. To further clarify the interaction of the complexes with DNA, a competitive binding experiment was carried out. The intrinsic fluorescence intensity of DNA is very low, and that of EB in Tris buffer is also not high due to quenching by the solvent molecules. However, EB emits intense fluorescence at about 600 nm in the presence of DNA due to its strong intercalation between the adjacent DNA base pairs [52]. It was previously reported that the enhanced fluorescence could be quenched by addition of another molecule [53]. Thus, EB can be used to probe the interaction of complexes with DNA. The relative binding of **1**–**7** to CT-DNA was studied with an EB-bound CT-DNA solution in 5 mM Tris-HCl/50 mM NaCl buffer (pH = 7.2) in figure S2. Fluorescence intensities (510 nm excitation) were measured at different complex concentrations. The extent of reduction of the emission intensity gives a measure of the binding propensity of the complex to DNA. In order to understand quantitatively the magnitude of the binding strength of the complexes with

CT-DNA, the classical Stern–Volmer equation is employed [54], $I_0/I = 1 + K$ [Q], where I_0 and I represent the fluorescence intensities in the absence and presence of quencher, Q is the concentration of quencher and K is a linear Stern–Volmer quenching constant. As shown in figure S2, the quenching plot illustrates that the quenching of EB bound to DNA by the complex is in agreement with the linear Stern–Volmer equation, which also indicates that the complex binds to DNA. In the plot of I_0/I *versus* [complex], K is given by the ratio of the slope to intercept. According to the equation K_{EB} [EB] = K_{app} [complex], where the complex concentration is the value at a 50% reduction of the fluorescence intensity of EB and $K_{EB} = 1.0 \times 10^7$ M^{-1} ([EB] = 50 μM). The apparent binding constant (K_{app}) values were calculated to be 5.2×10^5 M^{-1} for **1**, 1.05×10^5 M^{-1} for **2**, 5.76×10^5 M^{-1} for **3**, 4.57×10^5 M^{-1} for **4**, 1.29×10^5 M^{-1} for **5**, 1.7×10^5 M^{-1} for **6**, 2.53×10^5 M^{-1} for **7**, the binding propensity to the calf thymus DNA in the order: **3** (Co-phen) > **1** (Zn-phen) > **4** (Ni-phen) > **7** (Cd-phen) > **6** (Ni-dafo) > **5** (Ni-bpy) > **2** (Zn-bpy), less than the binding constant of the classical intercalators and metallo intercalators (10^7 M^{-1}, which was reported by Cory *et al.* [55]), which suggests that the interaction of **1**–**7** with DNA is a moderate intercalative mode. The DNA binding affinity is due to the involvement in partial insertion of the aromatic ring in ancillary ligands (phen>dafo>bpy) between DNA base pairs. Such quenched fluorescence of EB bound to DNA is also found in other binuclear complexes and the K_{app} values are similar [56, 57].

3.2.3. Circular dichroism studies. CD spectroscopy is useful in monitoring the conformational variations of DNA in solution and provides detailed information about the binding of the complex with DNA. The CD spectrum of calf thymus (CT-DNA) exhibits a positive band at 275 nm due to base stacking and a negative band at 245 nm due to the helicity of B-type DNA [58]. Figure S3 displays the CD spectra of calf thymus (CT-DNA) in the absence and presence of **1**–**7**. For **2**–**7**, both the positive (~275 nm) and negative (~245 nm) bands decrease in intensity on addition of complex. The decreased intensity in the negative band suggests the complex can unwind the DNA helix and lead to loss of helicity [59]. For **1**, the positive band (~275 nm) increased in intensity on addition of complex, while the negative (~245 nm) band decreased in intensity, indicating that the DNA binding of the complex induces base stacking and enhances the stability of DNA [60].

3.2.4. Viscosity measurements. Due to its sensitivity to the change of length of DNA, viscosity measurement may be the most effective means to study the binding mode of the complex to DNA, especially in the absence of crystallographic structure data. A significant increase in the viscosity of DNA on addition of the complex indicates the classical intercalative mode of binding to DNA. In contrast, a complex that binds in the DNA grooves by partial and/or non-classical intercalation causes less pronounced (positive or negative) or no change in DNA solution viscosity [61]. Viscosity measurements were carried out on calf thymus (CT-DNA) by varying the concentration of the complex. Figure 2 shows **2**–**7** cause a decrease in the relative viscosity of DNA, while an increase for **1**; this may be explained by a binding mode which produced bends or kinks in the DNA and thus reduced its effective length and concomitantly its viscosity for **2**–**7**, while the insertion of **1** in between the DNA base pairs, leading to an increase in the separation of base pairs at intercalation sites and, thus, an increase in overall DNA contour length. This result is consistent with that of the circular dichroism studies.

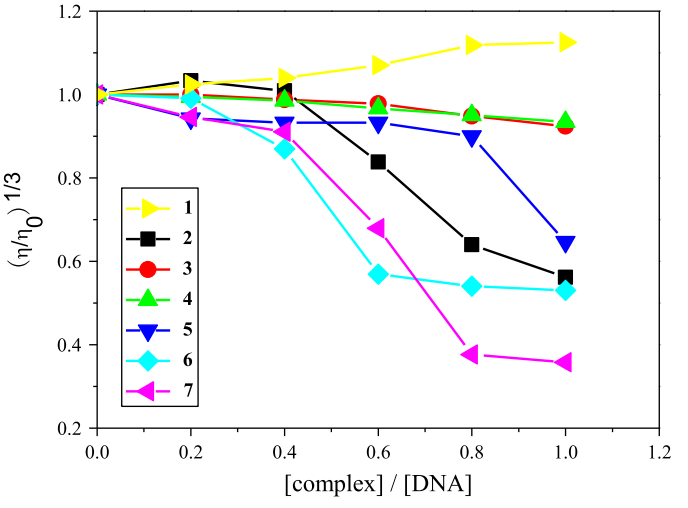

Figure 2. Effect of increasing amounts of **1**–**7** on the relative viscosity of calf thymus DNA at 37 (± 0.1) °C in 5 mM Tris-HCl buffer (pH = 7.2, [DNA] = 0.1 mM).

3.3. *pBR322 DNA cleavage by 1–7*

To assess the chemical nuclease activities of **1**–**7** for DNA strand scission, pBR322 DNA was incubated with the seven complexes under the reaction conditions. The cleavage reaction can be monitored by gel electrophoresis. When circular pBR322 DNA is subjected to electrophoresis, relatively fast migration will be observed for the intact supercoiled form (Form I). If scission occurs on one strand (nicking), the supercoiled form will relax to generate a slower-moving nicked form (Form II). If both strands are cleaved, a linear form (Form III) that migrates between Form I and Form II will be generated.

3.3.1. Effects of complex concentration on plasmid DNA cleavage. First, the chemical nuclease activities of **1**–**7** have been studied using supercoiled pBR322 plasmid DNA as a substrate in a medium of 50 mM Tris-HCl/NaCl buffer (pH = 7.2) in the presence of activators (here are hydrogen peroxide and hydrogen peroxide/ascorbate) under physiological conditions. The DNA cleavage activity of the complexes was assayed by the conversion of supercoiled DNA (Form I) to nicked circular (Form II) or linearized DNA (Form III). As shown in figure 3, control experiments using only hydrogen peroxide or hydrogen peroxide/ascorbate did not show any significant DNA cleavage under similar experimental conditions (lane 2 and lane 8), with increasing concentration of the complexes; the supercoiled DNA decreases and nicked form gradually increases. The results indicate that the DNA cleavage activity of the complexes is obviously concentration-dependent. Since **1** shows low nuclease activity at higher concentration, it may be attributed to the condensation between the complex and DNA, so as to induce the interaction with DNA [62]. The linear form (Form III) appears significantly for Zn(II) complexes **1** and **2** and Cd(II) complex **7**, while it is not for other complexes under the experimental condition.

From figure 3, we also see that the seven complexes all show higher nuclease activity in the presence of 0.25 mM H_2O_2/ascorbate than that of 0.25 mM H_2O_2, indicating that the cleavage activity of **1**–**7** is related to the amount of the activator, for which Zn(II) and

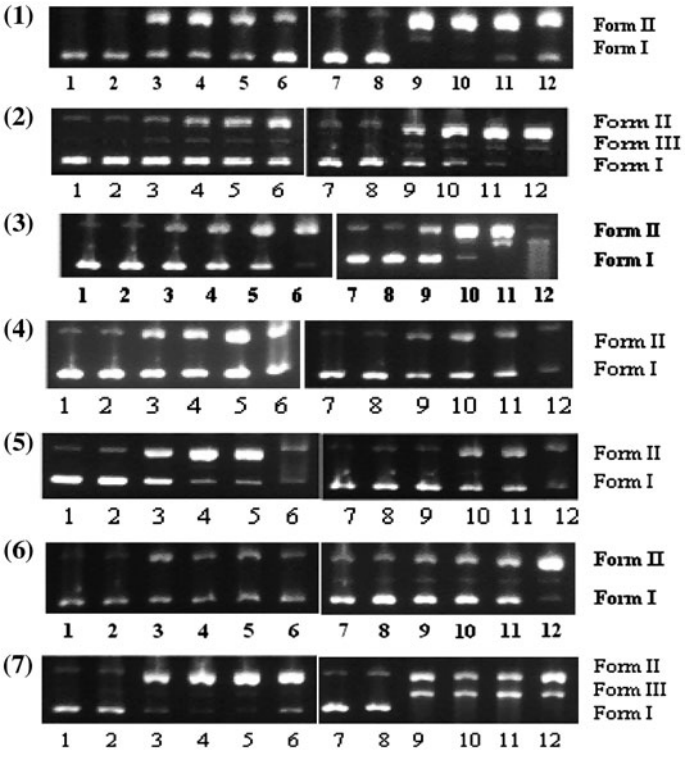

Figure 3. Gel electrophoresis diagrams showing cleavage of pBR322 DNA (0.1 μg/μL) in the presence of external agents at different complex concentrations in Tris-HCl/NaCl buffer (pH = 7.2) and 37 °C for 3 h. (**1**) Lane 1: DNA control (3 h); lane 2: DNA + 0.25 mM H_2O_2; lanes 3-6: DNA + 0.25 mM H_2O_2 + **1** (0.005, 0.01, 0.015, 0.02 mM); lane 7: DNA control; lane 8: DNA + 0.25 mM H_2O_2/ascorbate; lanes 9–12: DNA + 0.25 mM H_2O_2/ascorbate + **1** (0.005, 0.01, 0.015, 0.02 mM); (**2**) lane 1: DNA control (3 h); lane 2: DNA + 0.25 mM H_2O_2; lanes 3–6: DNA + 0.25 mM H_2O_2 + **2** (0.005, 0.01, 0.015, 0.02 mM); lane 7: DNA control; lane 8: DNA + 0.25 mM H_2O_2/ascorbate; lanes 9–12: DNA + 0.25 mM H_2O_2/ascorbate + **2** (0.005, 0.01, 0.015, 0.02 mM); (**3**) lane 1: DNA control; lane 2: DNA + 0.25 mM H_2O_2; lanes 3–6: DNA + 0.5 mM H_2O_2 + **3** (0.005, 0.02, 0.035, 0.05 mM); lane 7: DNA control; lane 8: DNA + 0.25 mM H_2O_2/ascorbate; lanes 9–12: DNA + 0.25 mM H_2O_2/ascorbate + **3** (0.005, 0.025, 0.05, 0.075 mM); (**4**) lane 1: DNA control; lane 2: DNA + 0.25 mM H_2O_2; lanes 3–6: DNA + 0.25 mM H_2O_2 + **4** (0.005, 0.025, 0.05, 0.25 mM); lane 7: DNA control; lane 8: DNA + 0.25 mM H_2O_2/ascorbate; lanes 9–12: DNA + 0.25 mM H_2O_2/ascorbate + **4** (0.005, 0.025, 0.05, 0.1 mM); (**5**) lane 1: DNA control; lane 2: DNA + 0.25 mM H_2O_2; lanes 3–6: DNA + 0.25 mM H_2O_2 + **5** (0.005, 0.025, 0.05, 0.25 mM); lane 7: DNA control; lane 8: DNA + 0.25 mM H_2O_2/ascorbate; lanes 9–12: DNA + 0.25 mM H_2O_2/ascorbate + **5** (0.005, 0.025, 0.05, 0.1 mM); (**6**) lane 1: DNA control; lane 2: DNA + 0.25 mM H_2O_2; lanes 3–6: DNA + 0.25 mM H_2O_2 + **6** (0.005, 0.02, 0.035, 0.05 mM); lane 7: DNA control; lane 8: DNA + 0.25 mM H_2O_2/ascorbate; lanes 9–12: DNA + 0.25 mM H_2O_2/ascorbate + **6** (0.005, 0.01, 0.015, 0.025 mM); (**7**) lane 1: DNA control; lane 2: DNA + 0.25 mM H_2O_2; lanes 3–6: DNA + 0.25 mM H_2O_2 + **7** (0.005, 0.01, 0.015, 0.02 mM); lane 7: DNA control; lane 8: DNA + 0.25 mM H_2O_2/ascorbate; lanes 9–12: DNA + 0.25 mM H_2O_2/ascorbate + **7** (0.005, 0.01, 0.015, 0.02 mM).

Cd(II) complexes show obviously higher cleavage activity than that of Co(II) and Ni(II) complexes under the conditions chosen for our experiments. The oxidative cleavage activity of the complexes is not readily correlated to the binding propensity, but this may be related to the mechanism of DNA cleavage by complexes. Several authors have studied the influence of different activators on the cleavage of DNA by binuclear complexes [63–65]. Sigman *et al.* [63] have found MPA to be superior to ascorbate as an activating agent on the nuclease activity of a bis (o-phenanthroline)-copper(II) complex because it produces less

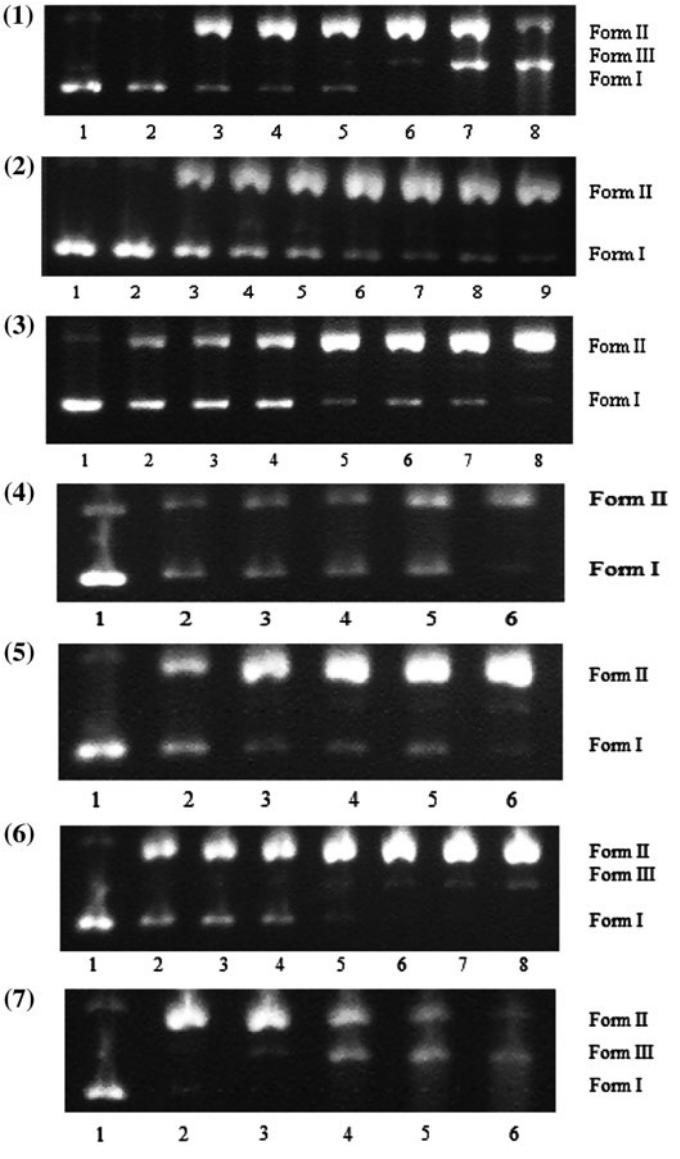

Figure 4. Time-dependence of pBR322 DNA cleavage by complexes in Tris-HCl/NaCl buffer (pH = 7.2) at 37 °C. (**1**) Lane 1: DNA control (4 h), lanes 2–8: DNA + 0.25 mM H_2O_2 + 0.025 mM **1** (0, 0.17, 0.5, 1, 2, 3, 4 h), respectively; (**2**) lane 1: DNA control (3 h), lanes 2–9: DNA + 0.25 mM H_2O_2 + 0.03 mM **2** (0, 10, 20, 30, 40, 60, 120, 180 min), respectively; (**3**) lane 1: DNA control (5 h), lanes 2–8: DNA + 0.25 mM H_2O_2 + 0.05 mM **3** (0.17, 0.5, 1, 2, 3, 4, 5 h), respectively; (**4**) lane 1: DNA control (5 h), lanes 2–6: DNA + 0.25 mM H_2O_2/ascorbate + 0.1 mM **4** (0.5, 1, 2, 3, 5 h), respectively; (**5**) lane 1: DNA control (4 h), lanes 2–6: DNA + 0.25 mM H_2O_2/ascorbate + 0.05 mM **5** (0.5, 1, 2, 3, 4 h), respectively; (**6**) lane 1: DNA control (6 h), lanes 2–8: DNA + 0.25 mM H_2O_2/ascorbate + 0.025 mM **6** (0.5, 1, 2, 3, 4, 5, 6 h), respectively; (**7**) lane 1: DNA control (5 h), lanes 2–6: DNA + 0.25 mM H_2O_2/ascorbate + 0.01 mM **7** (0.5, 1, 2, 3, 5 h), respectively.

background cleavage. Chiou *et al.* [64] have showed that ascorbate is more effective in cleaving DNA than other reducing agents such as MPA and dithiothreitol due to its ability

to generate hydrogen peroxide in the presence of oxygen and metal ions, whereas other reducing agents are known to produce superoxide, which rapidly undergoes dismutation in aqueous solution. Detmer *et al.* [65] have indicated that a mixture of hydrogen peroxide and ascorbate is a more effective activating agent than ascorbate alone. In our work, we have found that hydrogen peroxide/ascorbate is the best activator for DNA cleavage.

3.3.2. Effects of reaction time on plasmid DNA cleavage. The time-dependent DNA cleavage by **1**–**7** was also studied. Figure 4 shows the results of gel electrophoretic separations of plasmid pBR322 DNA induced by increasing reaction time in the presence of external agents at pH = 7.2 (50 mM Tris–HCl/NaCl buffer) and 37 °C. With reaction time increasing, the amount of Form II increases and Form I gradually disappears; Form III also appears significantly for **1** and **7** obviously. The results show that **1**–**7** can effectively cleave the pBR322 plasmid DNA in the presence of external agent, and the cleavage of DNA by the complexes is dependent on the reaction time.

3.3.3. Effects of radical scavengers on plasmid DNA cleavage. Most metallonucleases cleave DNA through oxidative process due to their containing redox potential of metal ions. The complexes have been shown to react with molecular oxygen or hydrogen peroxide to produce a variety of active oxidative intermediates (reactive oxygen species or nondiffusible metal-oxene species). In order to obtain information about the active oxygen species which was responsible for the DNA damage, we have investigated the DNA cleavage in the presence of hydroxyl radical scavengers (DMSO and EtOH), singlet oxygen quenchers (NaN_3, L-Histidine, KI), superoxide scavenger (superoxide dismutase enzyme SOD), and hydrogen peroxide scavenger (catalase).

From figure S4, we see that the addition of NaN_3 inhibits the cleavage activity, which is indicative of the involvement of singlet oxygen or a singlet oxygen-like entity in the cleavage process for the seven complexes. The inhibitory activity of sodium azide can be ascribed to the affinity of the azide anion for transition metals [66]. This also can be seen from the obvious inhibition of addition of potassium iodide for **3**, **4** and **6**. For **5** and **6** the DMSO, EtOH, SOD enzyme and catalase also have an influence on the DNA cleavage, suggesting that the hydroxyl radical, superoxide anion and hydrogen peroxide are involved in the process. For **1**, **2** and **7** the addition of L-Histidine could not absolutely inhibit the cleavage DNA activity of the three complexes, the Zn(II)/H_2O_2 and Cd(II)/H_2O_2 systems can efficiently cleavage DNA due to that the peroxide ion coordinated to the Zn(II) and Cd(II) ions enhanced their nuleophilicity [67–69]. In order to assure the sites of interaction between the complexes and DNA, we added the SYBR Green and methyl green, which are known to interact with DNA at minor and major grooves [70, 71]. The addition of SYBR Green could inhibit DNA cleavage by **3**, **5**, **6** and **7**; the result suggests that the four complexes mainly have interaction with DNA through the minor groove.

4. Conclusion

We have synthesized and characterized redox and non-redox active metal complexes with 1,4-tpbd ligand and a coligand. The complexes can all cleave plasmid DNA in the presence of external agents. DNA cleavage mechanism studies show that the complexes examined here may be capable of promoting DNA cleavage through an oxidative DNA damage

pathway. We have found that the cleavage activities of these complexes are related to metal ions and cleavage mechanism. Interestingly, here the Zn(II) and Cd(II) complexes show oxidative DNA cleavage through a hydrolytic cleavage process, this is rare.

Supplementary material

DNA binding assays, such as UV absorption spectra, emission spectra CD spectra, viscosity, and DNA cleavage by the complexes in the presence of various additives. Crystallographic data in CIF format and check CIF for **1**–**7**.

Funding

Project supported by China Postdoctoral Science Foundation [number 2011M500526].

References

[1] M.E. Núñez, J.K. Barton. *Curr. Opin. Chem. Biol.*, **4**, 199 (2000).
[2] S.E. Wolkenberg, D.L. Boger. *Chem. Rev.*, **102**, 2477 (2002).
[3] T.D. Tullius, J.A. Greenbaum. *Curr. Opin. Chem. Biol.*, **9**, 127 (2005).
[4] J.D. West, L.J. Marnett. *Chem. Res. Toxicol.*, **19**, 173 (2006).
[5] Q. Jiang, N. Xiao, P.F. Shi, Y.G. Zhu, Z.J. Guo. *Coord. Chem. Rev.*, **251**, 1951 (2007).
[6] W.K. Pogozelski, T.D. Tullius. *Chem. Rev.*, **98**, 1089 (1998).
[7] C.J. Burrows, J.G. Muller. *Chem. Rev.*, **98**, 1109 (1998).
[8] M. Costas, M.P. Mehn, M.P. Jensen, L. Que Jr. *Chem. Rev.*, **104**, 939 (2004).
[9] G. Parkin. *Chem. Rev.*, **104**, 699 (2004).
[10] A.J. Wu, J.E. Penner-Hahn, V.L. Pecoraro. *Chem. Rev.*, **104**, 903 (2004).
[11] D.C. Crans, J.J. Smee, E. Gaidamauskas, L. Yang. *Chem. Rev.*, **104**, 849 (2004).
[12] L.M. Mirica, X. Ottenwaelder, T.D.P. Stack. *Chem. Rev.*, **104**, 1013 (2004).
[13] M. González-Álvarez, G. Alzuet, J. Borrás, B. Macías, A. Castiñeiras. *Inorg. Chem.*, **42**, 2992 (2003).
[14] W.J. Pogozelski, T.J. McNeese, T.D. Tullius. *J. Am. Chem. Soc.*, **117**, 6428 (1995).
[15] D.S. Sigman. *Acc. Chem. Res.*, **19**, 180 (1986).
[16] R.M. Burger. *Chem. Rev.*, **98**, 1153 (1998).
[17] C.A. Claussen, E.C. Long. *Chem. Rev.*, **99**, 2797 (1999).
[18] B. Mestre, A. Jakobs, G. Pratviel, B. Meunier. *Biochemistry*, **35**, 9140 (1996).
[19] Y.Y. Fang, C.A. Claussen, K.B. Lipkowitz, E.C. Long. *J. Am. Chem. Soc.*, **128**, 3198 (2006).
[20] J.L. Czlapinski, T.L. Sheppard. *Chem. Commun.*, **2468**, (2004).
[21] K.J. Humphreys, K.D. Karlin, S.E. Rokita. *J. Am. Chem. Soc.*, **124**, 8055 (2002).
[22] Y. Zhao, J. Zhu, W. He, Z. Yang, Y. Zhu, Y. Li, J. Zhang, Z. Guo. *Chem. Eur. J.*, **12**, 6621 (2006).
[23] P.D. Hoog, L.D. Pachón, P. Gamez, M. Lutz, A.L. Spek, J. Reedijk. *Dalton Trans.*, 2614 (2004).
[24] P.U. Maheswari, S. Barends, S. Özalp-Yaman, P.D. Hoog, H. Casellas, S.J. Teat, C. Massera, M. Lutz, A.L. Spek, G.P.V. Wezel, P. Gamez, J. Reedijk. *Chem. Eur. J.*, **13**, 5213 (2007).
[25] A.T. Tan, R.C. Woodworth. *Biochemistry*, **8**, 3711 (1969).
[26] D.L. Hamilton, L.S. Valberg. *Am. J. Physiol.*, **227**, 1033 (1974).
[27] Z. Hossain, F. Huq. *J. Inorg. Biochem.*, **90**, 85 (2002).
[28] D.C. Lemkuil, D. Nettesheim, C.F. Shaw, D.H. Petering. *J. Biol. Chem.*, **269**, 24792 (1994).
[29] N.A. Illán-Cabeza, R.A. Vilaplana, Y. Alvarez, K. Akdi, S. Kamah, F. Hueso-Ureña, M. Quirós, F. González-VÍlchez, M.N. Moreno-Carretero. *J. Biol. Inorg. Chem.*, **10**, 924 (2005).
[30] J.M. Pérez, V. Cerrillo, A.I. Matesanz, J.M. Millán, P. Navarro, C. Alonso, P. Souza. *Chem. Biochem.*, **2**, 119 (2001).
[31] Z.S. Yang, J.S. Yu, H.Y. Chen. *Chin. J. Inorg. Chem.*, **18**, 373 (2002).
[32] T. Buchen, A. Hazell, L. Jessen, C.J. McKenzie, L.P. Nielsen, J.Z. Pedersen, D. Schollmeyer. *J. Chem. Soc., Dalton Trans.*, 2697 (1997).
[33] G.M. Sheldrick. *SHELXS 97*., University of Gottingen, Gottingen, Program for the Solution of Crystal Structures (1997).
[34] G.M. Sheldrick. *SHELXL 97*., University of Gottingen, Gottingen, Program for the Refinement of Crystal Structures (1997).

[35] J. Marmur. *J. Mol. Biol.*, **3**, 208 (1961).
[36] M.E. Reichmann, S.A. Rice, C.A. Thomas, P. Doty. *J. Am. Chem. Soc.*, **76**, 3047 (1954).
[37] G. Cohen, H. Eisenberg. *Biopolymers*, **8**, 45 (1969).
[38] Y. Gultneh, A.R. Khan, D. Blaise, S. Chaudhry, B. Ahvazi, B.B. Marvey, R.J. Butcher. *J. Inorg. Biochem.*, **75**, 7 (1999).
[39] W.H. Armstrong, S.J. Lippard. *J. Am. Chem. Soc.*, **106**, 4630 (1984).
[40] D.D. Li, J.L. Tian, Y.Y. Kou, F.P. Huang, G.J. Chen, W. Gu, X. Liu, D.Z. Liao, P. Cheng, S.P. Yan. *Dalton Trans.*, 3574 (2009).
[41] D.D. Li, F.P. Huang, G.J. Chen, C.Y. Gao, J.L. Tian, W. Gu, X. Liu, S.P. Yan. *J. Inorg. Biochem.*, **104**, 431 (2010).
[42] M. Baldini, M. Belicchi-Ferrari, F. Bisceglie. P.P. Dall'Aglio, G. Pelosi, S. Pinelli, P. Tarasconi, *Inorg. Chem.*, **43**, 7170 (2004).
[43] J.K. Barton, A.T. Danishefsky, J.M. Goldberg. *J. Am. Chem. Soc.*, **106**, 2172 (1984).
[44] S.A. Tysoe, R.J. Morgan, A.D. Baker, T.C. Strekas. *J. Phys. Chem.*, **97**, 1707 (1993).
[45] T.M. Kelly, A.B. Tossi, D.J. McConnell, T.C. Strekas. *Nucleic Acids Res.*, **13**, 6017 (1985).
[46] Y.G. Sun, K.L. Li, Z.H. Xu, T.Y. Lv, S.J. Wang, L.X. You, F. Ding. *J. Coord. Chem.*, **66**, 2455 (2013).
[47] Y.F. Chen, M. Liu, J.W. Mao, H.T. Song, H. Zhou, Z.Q. Pan. *J. Coord. Chem.*, **65**, 3413 (2012).
[48] N.V. Kulkarni, V.K. Revankar. *J. Coord. Chem.*, **64**, 725 (2011).
[49] N. Raman, K. Pothiraj, T. Baskaran. *J. Coord. Chem.*, **64**, 3900 (2011).
[50] F. Zhang, Q.Y. Lin, W.D. Liu, P.P. Wang, W.J. Song, B.W. Zheng. *J. Coord. Chem.*, **66**, 2297 (2013).
[51] R. Prabu, A. Vijayaraj, R. Suresh, R. Senbhagaraman, V. Kaviyarasan, V. Narayanan. *J. Coord. Chem.*, **66**, 206 (2013).
[52] F.J. Meyer-Almes, D. Porschke. *Biochemistry*, **32**, 4246 (1993).
[53] B.C. Baguley, M. LeBret. *Biochemistry*, **23**, 937 (1984).
[54] J.R. Lakowicz, G. Webber. *Biochemistry*, **12**, 4161 (1973).
[55] M. Cory, D.D. McKee, J. Kagan, D.W. Henry, J.A. Miller. *J. Am. Chem. Soc.*, **107**, 2528 (1985).
[56] D.D. Li, H.H. Zeng. *Appl. Organomet. Chem.*, **27**, 89 (2013).
[57] D.D. Li, J.L. Tian, W. Gu, X. Liu, H.H. Zeng, S.P. Yan. *J. Inorg. Biochem.*, **105**, 894 (2011).
[58] A. Rajendran, B.U. Nair. *Biochim. Biophys. Acta*, **1760**, 1794 (2006).
[59] K. Karidi, A. Garoufis, N. Hadjiliadis, J. Reedijk. *Dalton Trans.*, 728 (2005).
[60] J.G. Collins, T.P. Shields, J.K. Barton. *J. Am. Chem. Soc.*, **116**, 9840 (1994).
[61] T.M. Kelly, A.B. Tossi, D.J. McConnell, T.C. Strekas. *Nucleic Acids Res.*, **13**, 6017 (1985).
[62] R. Ren, P. Yang, W. Zheng, Z. Hua. *Inorg. Chem.*, **39**, 5454 (2000).
[63] A. Mazumder, C.L. Sutton, D.S. Sigman. *Inorg. Chem.*, **32**, 3516 (1993).
[64] S.H. Chiou, N. Ohtsu, K.G. Bensch, in: D. Karlin, J. Zubieta (Eds.), *Biological and Inorganic Copper Chemistry*, Adenine Press, New York (1985), p.119.
[65] C.A. Detmer III, F.V. Pamatong, J.R. Bocarsly. *Inorg. Chem.*, **35**, 6292 (1996).
[66] K.J. Humphreys, K.D. Karlin, S.E. Rokita. *J. Am. Chem. Soc.*, **124**, 8055 (2002).
[67] E.L. Hegg, J.N. Burstyn. *Inorg. Chem.*, **35**, 7474 (1996).
[68] J. Qian, W. Gu, H. Liu, F.X. Gao, L. Feng, S.P. Yan, D.Z. Liao, P. Cheng. *Dalton Trans.*, 1060 (2007).
[69] J. He, J. Sun, Z.W. Mao, L.N. Ji, H.Z. Sun. *J. Inorg. Biochem.*, **103**, 851 (2009).
[70] D. Gibellini, F. Vitone, P. Schiavone, C. Ponti, M.L. Placa, M.C. Re. *J. Clin. Virol.*, **29**, 282 (2004).
[71] F.B. El Amrani, L. Perelló, J.A. Real, M. González-Alvarez, G. Alzuet, J. Borrás, S. García-Granda, J. Montejo-Bernardo. *J. Inorg. Biochem.*, **100**, 1208 (2006).